X-ray diffraction from laterally structured surfaces: Total external reflection

M. Tolan and W. Press

Institut für Experimentalphysik, Christian-Albrechts-Universität Kiel, Olshausenstrasse 40, 24098 Kiel, Germany

F. Brinkop and J. P. Kotthaus

Sektion Physik, Ludwig-Maximilians-Universität München, Geschwister-Scholl-Platz 1, 80539 München, Germany

In this work x-ray-diffraction measurements from GaAs surface gratings are presented. The experiments were performed using a three-crystal diffractometer. Measurements in the region of total external reflection (small incidence angles) for five samples were done and compared with model calculations based on a dynamical scattering theory. The theory is able to explain all experiments quantitatively. Mesoscopic grating parameters as well as microscopic surface roughnesses of the samples were obtained from fits of the data. For three samples scanning-electron-microscope pictures were taken. The analysis of these pictures leads to the same mesoscopic parameters as obtained from x-ray diffraction.

I. INTRODUCTION

It is well known that x-ray diffraction becomes surface sensitive in the case of small incident angles (for a review, see, e.g., Ref. 1). The real part of the refractive index is slightly smaller than 1 and therefore total external reflection occurs at grazing incidence angles.[2] In this region the penetration depth of the incoming waves is relatively small and the scattered intensities mainly contain information about the structure of the near-surface region. X-ray diffraction, in particular x-ray reflectivity, is able to yield a density profile of the sample in a nondestructive manner. In contrast to crystal-truncation-rod[3–5] investigations near Bragg reflections, total-external-reflection measurements are not sensitive to the crystalline structure of the surface or bulk material.

The x-ray reflectivity of a layer system is described by the well-known Parrat formalism including the effect of total external reflection which is based on the solution of a simple recurrence relation.[6–13] In the case of rough interfaces, the recurrence formula is modified depending on the particular roughness distribution perpendicular to the surfaces.[14–16] Additionally, the roughness causes nonspecular scattering (so-called diffuse scattering) which contains information about the lateral structure of the surface. Many works have focused on this topic within the last six years and great successes in explaining the data have been achieved.[9,16–26]

By slicing an arbitrary density profile into many uniform thin layers of constant electron density, the Parrat formalism is also able to give the reflectivity for more complex systems (see, e.g., Refs. 12 and 13). Bahr *et al.*[9] and Lurio *et al.*[27] clearly show that x-ray reflectivity is an extremely sensitive tool for investigating the particular shape of the density profile of a thin film perpendicular to the surface.

In this work, x-ray-diffraction measurements within the region of total external reflection from *laterally* structured surfaces (i.e., surface gratings) are presented. These samples contain mesoscopic length scales parallel *and*

perpendicular to the surface (lateral periods in the range of micrometers, heights of about 0.1 μm) as well as microscopic length scales (roughness). Furthermore, these gratings can be regarded as a particular "rough" surface with some enhanced Fourier components.

Previous work concerning x-ray diffraction from laterally structured surfaces was done by Aristov *et al.*,[28–30] Macrander and Slusky,[31] Tapfer *et al.*,[32,33] van der Sluis, Binsma, and van Dongen,[34] Gailhanou *et al.*,[35] Shen *et al.*,[36] Holý *et al.*,[37] and Tolan *et al.*[5] All these papers deal with the influence of crystalline mesoscopic surface gratings on the diffracted intensities in the vicinity of Bragg reflections. Therefore dynamical scattering theory can be avoided in almost all cases and the simple kinematical Born approximation is valid (a nice example of effects which cannot be explained within the Born approximation is given in the work of Gailhanou *et al.*[35]).

But in the region of total external reflection, multiple-scattering effects are dominant and the kinematical approach is not valid. Unfortunately, it is not possible to adopt the distorted-wave Born approximation (DWBA), introduced by Sinha *et al.*[17] to describe the diffuse scattering from a rough surface, to surface gratings because these structures cannot be treated as a small perturbation of a smooth surface. Also, the existing theories for longer wavelengths of the incident radiation (i.e., soft x-rays up to visible light; for a review, see Ref. 38) are unable to describe the scattering from laterally structured surfaces because approximations and assumptions were used which are not valid for hard x rays.

Therefore we have developed a dynamical theory for x-ray diffraction from mesoscopic surface gratings. This theory is able to describe our measurements quantitatively. Mesoscopic parameters of the particular surface contour and microscopic information like the surface roughness can be obtained from fits to the data. A short account of this topic was already given in a recent paper.[39]

The present paper is structured as follows. After the Introduction the samples are described. Next the dynam-

ical scattering theory for rough, arbitrarily shaped, laterally structured surfaces is shown. Then a brief description of the setup of the three-crystal diffractometer (TCD) follows. After that the measurements as well as the fit results are presented in detail. Conclusions and an outlook finish this paper.

II. SAMPLES

The samples which were investigated are five GaAs(001) surface gratings. They were prepared with photolithographic methods. First a layer of photoresist was deposited on top of the molecular-beam-epitaxy (MBE) -grown GaAs(001) surface. Then a laser interference pattern defines the lateral structure. Finally the exposed parts were wet etched with a 20:1:1 H_2O-H_2O_2-H_2SO_4 solution and afterwards the photoresist was removed from the surface (for details, see Refs. 40–43). Figure 1 shows schematically a sketch of such a grating. A scanning-electron-microscope (SEM) picture yields a symmetric trapezoidal shape of the surface contour with well-defined bars of length s and grooves of length g.

Whereas the lateral grating period d only depends on the laser wavelength and the interference angle, the other parameters strongly depend on the etching process. In particular, the grating height h can be estimated with the etching ratio $r \approx 50$ Å/s and the respective etching time t_{etch} to $h \sim r t_{etch}$.

After the x-ray measurements three samples $S1$, $S2$, and $S4$ were cleaved and investigated with a SEM to compare the x-ray results with the directly observed grating pictures. Table I shows the parameters of the samples $S1$–$S5$ which were known from the preparation processes and the SEM pictures. A quantitative comparison of these pictures with the x-ray results is given in Sec. V.

In the soft-x-ray range surface gratings are used as monochromators (see Refs. 44 and 45) whereas etched surface contours like Fresnel lenses are used as optical elements to focus hard x rays.[46,47] The surface gratings which were investigated in this work are prepared quite similarly to those employed to create low-dimensional quantum systems by etching[48] or direct growth on patterned substrates.[49] With the technique described above, one-dimensional (quantum wires) as well as zero-dimensional (quantum dots) quantum systems can be realized and the electronic properties of such systems were the topic of many research works in recent years (see, for example, Refs. 42, 43, and 50–52, and references therein).
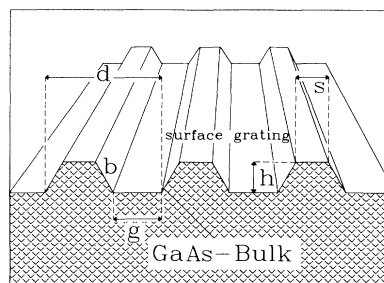

FIG. 1. Sketch of a symmetric trapezoidal surface grating with the width s of the bars, the width g of the grooves, the width b of the intermediate regions, the grating period d, and the height h.

But in the present work concerning surface x-ray scattering under total-external-reflection conditions only the geometrical structure is of interest.

III. THEORY

In this section the dynamical scattering theory for laterally structured surfaces will be presented in detail. Throughout this paper the following notation is used. The wave vectors of the incident and diffracted x-ray beam are $\mathbf{k}_i$ and $\mathbf{k}_f$ with $k_i = k_f = 2\pi/\lambda$ and the momentum transfer $\mathbf{q}$ is defined by $\mathbf{q} = \mathbf{k}_f - \mathbf{k}_i = (q_x, q_z)^T$. The scattering plane is the (x, z) plane (y denotes the out-of-plane direction), and ϑ_i and ϑ_f are the incident and exit angles, respectively, of the x-ray beam.

The function $f(x)$ describes the shape of a one-dimensional surface grating and has to fulfill the conditions $0 \leq f(x) \leq h$ and $f(x) = f(x + d)$ with the mesoscopic grating height h and the lateral period d. Furthermore, the region above the grating, i.e., $z > f(x)$, is denoted by $R_>$ and $R_<$ is the region below the surface structure ($z < 0$ is the bulk region). Due to the fact that $f(x)$ does not depend on the coordinate y, all fields are y independent and therefore only two-dimensional vectors $\mathbf{r} = (x, z)^T$, and $\mathbf{k} = (k_x, k_z)^T$ need to be used in the following.

In the case of small incident angles ϑ_i and fixed wavelength λ (here always $\lambda = 1.54$ Å) the refractive index n can be expressed by the simple relation $n = 1 - (\delta + i\beta)$ with the optical constants δ (dispersion) and β (absorption). For hard x rays δ and β are positive quantities but for many common semiconductors their magnitudes are only of the order of 10^{-6} and 10^{-7}, respectively. The

TABLE I. Preparation parameters of the samples $S1$–$S5$. The height h was estimated from the etching ratio in the z direction $r \sim 50$ Å/s and the etching time t_{etch}.

	d (Å)	$h \sim r t_{etch}$ (Å)	Sample size (mm²)	SEM
$S1$	15 500	~1500	7×5	well-defined grating
$S2$	15 500	~1500	7×5	strongly varying parameters
$S3$	15 500	~2000	7×7	no SEM picture
$S4$	5 900	~500	6×6	well-defined grating
$S5$	5 900	~1000	6×6	no SEM picture

precise values for $\lambda=1.54$ Å and bulk GaAs are $\delta=14.45\times10^{-6}$ and $\beta=4.95\times10^{-7}$. The critical angle of total external reflection $\vartheta_i=\sqrt{2\delta}$ is $\vartheta_c=0.307°$ for bulk GaAs. The dispersion δ as well as β are proportional to the electron density ρ of the examined system. Therefore x-ray-reflectivity measurements within the region of total external reflection are sensitive to the density profile. For laterally structured surfaces the refractive index n depends not only on z (direction perpendicular to the surface) but also on the in-plane coordinate x. In particular, one gets

$$n(x,z)=\begin{cases}1 & \text{for } (x,z)\in R_> \\ 1-(\delta+i\beta) & \text{for } (x,z)\in R_< .\end{cases} \tag{1}$$

Let us now suppose that an electromagnetic wave with field vector

$$\mathbf{E}^{(i)}=\mathbf{E}_0e^{i(\omega t-\mathbf{k}_i\mathbf{r})}, \quad \mathbf{k}_i=(k_{xi},k_{zi})^T=(k_i\cos\vartheta_i,k_i\sin\vartheta_i)^T,$$

illuminates the surface contour $f(x)$ of the sample. Then the diffracted field $\mathbf{E}^{(d)}$ within the region $R_>$ is $\mathbf{E}^{(d)}=\mathbf{E}-\mathbf{E}^{(i)}$ where $\mathbf{E}$ denotes the total field. For the transmitted field $\mathbf{E}^{(t)}$ in the region $R_<$ the condition $\mathbf{E}^{(t)}=\mathbf{E}$ simply holds. Equivalent expressions can be obtained if the magnetic field vectors $\mathbf{H}^{(d,t,i)}$ are considered.

In the following, only the particular case $\mathbf{E}_0=(0,E_{0y},0)^T$ is investigated (s polarization). For hard x rays the Fresnel formulas become independent of the polarization of the incident radiation and the difference between the s and p cases is negligible.[6]

From now on the letter F denotes the y component of the electric field and the subscripts (d), (i), and (t) mark diffracted, incident, and transmitted fields. Then, after separating all time-dependent factors from the Maxwell equations, the Helmholtz equation for $F^{(d,t)}$ can easily be extracted (see, e.g., Ref. 38):

$$\Delta F^{(d,t)}+n^2(x,z)k_i^2F^{(d,t)}=0 , \tag{2}$$

with the refractive index $n(x,z)$ given by Eq. (1). The fields $F^{(d)}$ and $F^{(t)}$ as well as their derivatives $d/d\hat{n}$ normal to the surface must be continuous on the grating, i.e., the following boundary conditions must be fulfilled:

$$F^{(d)}(x,f(x))+F^{(i)}(x,f(x))=F^{(t)}(x,f(x)) , \tag{3}$$

$$\frac{dF^{(d)}}{d\hat{n}}\bigg|_{z=f(x)}+\frac{dF^{(i)}}{d\hat{n}}\bigg|_{z=f(x)}=\frac{dF^{(t)}}{d\hat{n}}\bigg|_{z=f(x)} . \tag{4}$$

Additionally the solutions of Eqs. (2)–(4) have to vanish for $z\to-\infty$ (absorption within the semi-infinite bulk) and they must be plane waves for $z\to+\infty$ (no influence of the surface structure).

Due to the periodicity of the function $f(x)$ the fields can be expanded into a Fourier series

$$F^{(d,t)}=\sum_m t_m^{(d,t)}(z)e^{-ik_{xm}x} , \tag{5}$$

with $k_{xm}=k_{xi}-2K_m$, $K_m=m\pi/d$ (m integer), and the coefficients $t_m^{(d,t)}(z)$.

Inserting the expansion (5) into Eq. (2) yields for the region $z>h$

$$F^{(d)}(x,z)=\sum_m B_m\Phi_m(x,z) , \tag{6}$$

with outgoing plane waves

$$\Phi_m(x,z)=e^{-i\{k_{xm}x+k_{zm}(z-h)\}} . \tag{7}$$

Within the region $z<0$ a similar expansion for the transmitted field is obtained:

$$F^{(t)}(x,z)=\sum_m B_m^{(t)}\Phi_m^{(t)}(x,z) , \tag{8}$$

$$\Phi_m^{(t)}(x,z)=e^{-i\{k_{xm}x-k_{zm}^{(t)}(z-h)\}} . \tag{9}$$

The z components of the wave vectors of the diffraction orders m are given by the terms $k_{zm}=(k_i^2-k_{xm}^2)^{1/2}$ and $k_{zm}^{(t)}=(n^2k_i^2-k_{xm}^2)^{1/2}$, respectively. The transmitted waves given by Eqs. (8) and (9) are all exponentially damped. Double-diffraction effects as described by Gailhanou et al.,[35] which take into account that the stepped surface acts simultaneously as reflection and transmission grating, were not observed in our experiments with the GaAs samples (see Sec. V). Therefore the transmitted orders need not be considered in all further calculations.

Equation (6) is the so-called Rayleigh expansion of the field above the grating.[53] In addition to the specular reflected beam ($m=0$) nonspecular diffraction orders ($m\neq0$) with wave vectors $\mathbf{k}_{fm}=(k_{xm},k_{zm})^T$ are obtained. From the definition of k_{xm} and k_{zm} follows the well-known grating formula for the diffraction angles ϑ_{fm}:

$$d(\cos\vartheta_i-\cos\vartheta_{fm})=m\lambda . \tag{10}$$

Note that only diffraction orders m fulfilling the condition $k_{xm}^2<k_i^2$ yield measurable intensities. All other orders lead to "evanescent waves" which are exponentially damped inside the sample and propagate parallel to the surface. Figure 2 explains this schematically. The intensities I_m of the diffraction orders can be obtained by calculating the Poynting vector
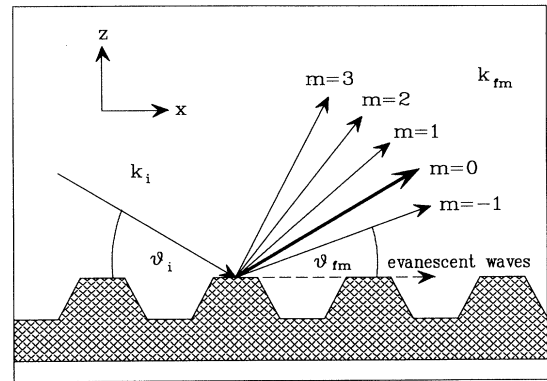

FIG. 2. By a periodic surface grating an incoming x-ray beam is also scattered in nonspecular directions (diffraction orders $m\neq0$). The evanescent waves are exponentially damped in the z direction and therefore they propagate parallel to the grating surface.

$$I_m = |B_m|^2 \frac{\sin\vartheta_{fm}}{\sin\vartheta_i} \ . \tag{11}$$

In particular, $|B_0|^2$ yields the reflectivity of the sample.

The real problem in calculating the diffracted intensities is the region $0 \le z \le h$. Rayleigh has made the assumption, the so-called Rayleigh hypothesis,[38,53] that the field $F^{(d)}(x,z)$ given by Eq. (6) is valid for *all* $(x,z) \in R_>$. The same assumption is made for the transmitted field $F^{(t)}(x,z)$ and the solution given by Eq. (8) is extended to the whole region $R_<$. If the Rayleigh hypothesis is valid the coefficients B_m and $B_m^{(t)}$ can be calculated by inserting the fields (6) and (8) into Eqs. (3) and (4). Then after dividing the interval $[0,d]$ into $2M+1$ points a linear system of equations for B_m and $B_m^{(t)}$ follows, which can easily be solved up to the order M (for details, see Ref. 38).

Unfortunately, numerical tests show that the Rayleigh hypothesis seems to be invalid for the problem discussed in this work. In the case of hard x rays shadowing effects (i.e., absorption effects) must be considered (note that $\lambda/h \sim 10^{-3}$, $\lambda/d \sim 10^{-4}$, and $h/d \sim 0.1$). These effects were neglected by making use of the Rayleigh hypothesis. Furthermore, the work of Maystre and Cadilhac[38,54] shows that in general it is not easy to decide if the Rayleigh hypothesis is valid or not.

Therefore we calculate the coefficients B_m in a different way. After some mathematics (for details, see Refs. 38 and 55) the following integral equation for B_m is obtained:

$$B_m = \frac{1}{2idk_{zm}} \int_{f(x)} \left\{ (F^{(d)} + F^{(i)})_> \frac{d\overline{\Phi}_{m>}}{d\hat{n}} \right. $$
$$\left. - \overline{\Phi}_{m>} \frac{d(F^{(d)} + F^{(i)})_>}{d\hat{n}} \right\} ds \ . \tag{12}$$

Here Φ_m is an outgoing plane wave with wave vector $\mathbf{k}_{fm}$ and the overbar denotes that the complex conjugate quantity has to be chosen. The index " $>$ " means that the respective limit from the region above the grating (i.e., from $R_>$) must be taken and the integral has to be performed over the shape $f(x)$ of the surface. Of course, Eq. (12) is not the solution of the whole problem because the fields $F^{(d,i)}$ as well as Φ_m are not known on the grating surface. Therefore we have to make an approximation to solve the problem. In zeroth order averaged fields on top of the grating have to be assumed. These fields will be inserted into Eq. (12) to obtain the intensities of the diffraction orders.

A surface grating function $f(x)$ with a flat region of width s and $f(x)=h$ ("bars"), another flat region of width g with $f(x)=0$ ("grooves"), and two intermediate regions of widths b_1 and b_2 will now be assumed ($d = g + b_1 + s + b_2$). The explicit form is given by [see also Fig. 3(a)]

$$f(x) = \begin{cases} 0, & 0 \le x < g \\ f_1(x), & g \le x < g + b_1 \\ h, & g + b_1 \le x < d - b_2 \\ f_2(x), & d - b_2 \le x < d \end{cases} \tag{13}$$

with arbitrary functions $f_1(x)$ and $f_2(x)$.

To obtain the zeroth-order approximation the electron density $\rho(x,z)$ is averaged over one grating period, i.e., the lateral structure is replaced by a density profile, $\rho(z) = \langle \rho(x,z) \rangle_x$ [Fig. 3(a)] with

$$\rho(z) = \frac{1}{d} \int_0^d \rho(x,z) dx$$

$$= \begin{cases} 0 & \text{for } z > h \\ \rho_{\text{bulk}} \dfrac{f_2^{-1}(z) - f_1^{-1}(z)}{d} & \text{for } 0 \le z \le h \\ \rho_{\text{bulk}} & \text{for } z < 0 \ . \end{cases} \tag{14}$$

Here ρ_{bulk} denotes the electron density of the bulk. The averaging process described by Eq. (14) is only justified if the spatial extent of the coherently illuminated area of
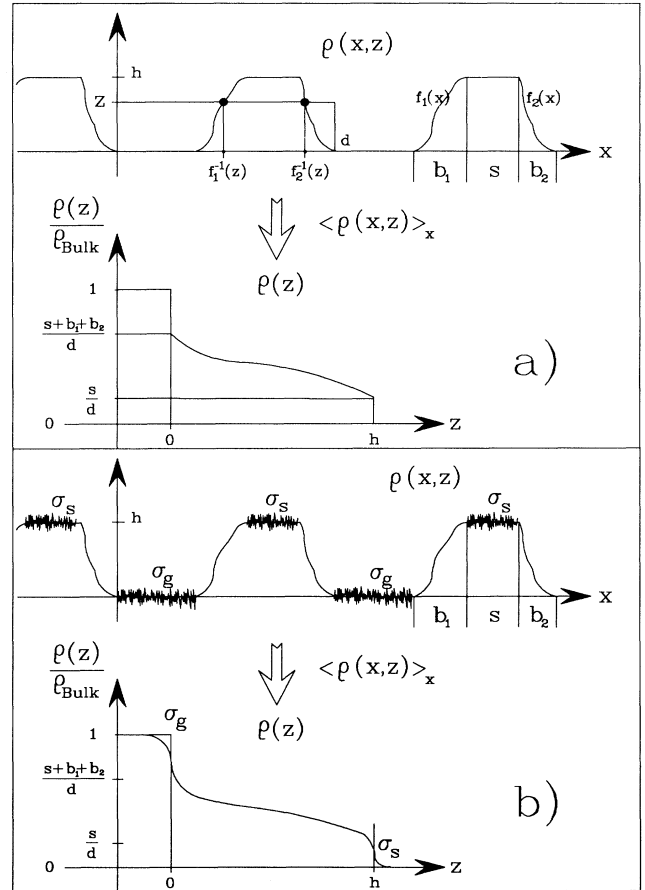

FIG. 3. (a) Smooth surface grating $f(x)$ with flat regions s and $g = d - b_1 - b_2 - s$, respectively, and arbitrarily shaped intermediate regions $b_{1,2}$ given by the functions $f_{1,2}(x)$. The two-dimensional density $\rho(x,z)$ is transformed into a one-dimensional averaged density function $\rho(z)$ (density-profile approximation). (b) Rough surface grating with the rms roughnesses σ_s and σ_g of the bars and grooves. Note that now the density profile $\rho(z)$ is more rounded at the z coordinates $z = 0$ and $z = h$.

the sample if much larger than the lateral periodicity d. An analysis of the respective coherence lengths shows that within the region of total external reflection this assumption is always valid (for details, see Refs. 55 and 56). Throughout this paper we will call the approximation given by Eq. (14) the "density-profile approximation."

From Eq. (14) a mean refractive index profile $n(z)$ follows:

$$n(z) = \langle n(x,z) \rangle_x$$

$$= \begin{cases} 1 & \text{for } z > h \\ 1 - (\delta + i\beta)\dfrac{\rho(z)}{\rho_{\text{bulk}}} & \text{for } 0 \le z \le h \\ 1 - (\delta + i\beta) & \text{for } z < 0 \end{cases} \qquad (15)$$

with the optical constants δ and β and the refractive index $n = 1 - (\delta + i\beta)$ of the bulk material (in this work always GaAs).

Now the zeroth-order approximation for the fields within the region $0 \le z \le h$, which are needed for calculating the coefficients B_m by inserting them into the right-hand side of Eq. (12), are

$$F^{(d)}(x,z) = R(z)e^{-i\{k_{xi}x + k_z(z)(z-h)\}}, \qquad (16)$$

$$F^{(i)}(x,z) = T(z)e^{-i\{k_{xi}x - k_z(z)(z-h)\}}, \qquad (17)$$

with the z-dependent k_z components

$$k_z(z) = k_i \sqrt{n^2(z) - \cos^2 \vartheta_i}, \qquad (18)$$

and two coefficients $R(z)$ and $T(z)$. These coefficients can be calculated using the well-known Parrat formalism[7] because the derivatives $d/d\hat{n}$ in Eq. (4) can be replaced by $\partial/\partial z$. The profile $\rho(z)$ is divided into N parts of constant electron density with the thickness $\varepsilon = h/N$. Furthermore, the continuous variable z is replaced by $z_j = j\varepsilon$ with the integer j ($j=0$ is the bulk and $j=N+1$ describes the vacuum region). With the conditions (3) and (4) the following recurrence formula is derived:[6]

$$X_{j+1} = \frac{R_{j+1}}{T_{j+1}} = e^{2ik_{z_{j+1}}(z_j - h)} \frac{\tilde{r}_{j+1,j} + X_j e^{-2ik_{z_j}(z_j - h)}}{1 + \tilde{r}_{j+1,j} X_j e^{-2ik_{z_j}(z_j - h)}}. \qquad (19)$$

Here $R_j = R(z_j)$, $T_j = T(z_j)$, $k_{z_j} = k_z(z_j)$, and the Fresnel coefficients of one (smooth) interface

$$\tilde{r}_{j+1,j} = (k_{z_{j+1}} - k_{z_j})/(k_{z_{j+1}} + k_{z_j})$$

were introduced. The starting point of the iteration is $R(0_<) = R_0 = 0$ (the index " $<$ " means that the limit has to be calculated from the bulk region, i.e., for $z \to -0$) and therefore $X_0 = 0$ because the substrate is assumed to be semi-infinite. Since $T_{N+1} = T(h+\varepsilon) = T(h_>) = 1$ (the amplitude of the incident wave is 1 for $z > h$) the amplitude of the reflected wave $R_{N+1} = R(h+\varepsilon) = R(h_>)$ can be obtained.

In contrast to the usual procedure for layer systems,

for surface gratings all other amplitudes R_j and T_j must also be calculated and afterwards inserted into the integral of Eq. (12) to obtain the coefficients B_m. The conditions (3) and (4) lead to the following equations for R_j and T_j:

$$R_j = \frac{1}{\tilde{t}_{j,j+1}} \{ T_{j+1}\tilde{r}_{j,j+1} e^{i(k_{z_j} + k_{z_{j+1}})(z_j - h)} + R_{j+1} e^{i(k_{z_j} - k_{z_{j+1}})(z_j - h)} \}, \qquad (20)$$

$$T_j = \frac{1}{\tilde{t}_{j,j+1}} \{ T_{j+1} e^{-i(k_{z_j} - k_{z_{j+1}})(z_j - h)} + \tilde{r}_{j,j+1} R_{j+1} e^{-i(k_{z_j} + k_{z_{j+1}})(z_j - h)} \}, \qquad (21)$$

with $j = N+1$, $R_{N+1} = R(h_>)$, and $T_{N+1} = T(h_>) = 1$ as start points and the Fresnel transmission of one (smooth) interface $\tilde{t}_{j,j+1} = 2k_{z_j}/(k_{z_j} + k_{z_{j+1}})$.

The field $\Phi_m(x,z)$ also has to be replaced by an averaged field within the region $0 \le z \le h$. By definition $\overline{\Phi}_m(x,z)$ should be the solution of the Helmholtz equation (see, e.g., Ref. 38)

$$\Delta \overline{\Phi}_m(x,z) + n^2(x,z)k_i^2 \overline{\Phi}_m(x,z) = 0, \qquad (22)$$

and additionally $\overline{\Phi}_m$ and $d\overline{\Phi}_m/d\hat{n}$ have to be continuous on the surface $z = f(x)$ of the grating.

Within the density-profile approximation, $n(x,z)$ in Eq. (22) has to be replaced by $\langle n(x,z) \rangle_x = n(z)$. Since $n(z) \equiv 1$ for $z > h$ one obtains

$$\overline{\Phi}(x,z) = \exp\{i[k_{xm}x + k_{zm}(z-h)]\}$$

[see Eq. (7)]. This plane wave describes a "time-reversed state" with wave vector $-\mathbf{k}_{fm} = (-k_{xm}, -k_{zm})^T$ (see Refs. 17 and 23). It is one possible final state for the scattering of the incident plane wave $F^{(i)}(x,z)$. Note that these final states for $m \ne 0$ exist in the case of a laterally structured surface. For uniform smooth layer systems only specular reflectivity is allowed.

Again, using the Parrat formalism yields the field $\overline{\Phi}_m(x,z)$ within the whole region $0 < z < h$. Therefore the following ansatz is chosen:

$$\overline{\Phi}_m(x,z) = \overline{\Phi}_T(x,z) + \overline{\Phi}_R(x,z), \qquad (23)$$

with

$$\overline{\Phi}_T(x,z) = T_{\Phi_m}(z)e^{i\{k_{xm}x + k_{zm}(z)(z-h)\}}, \qquad (24)$$

$$\overline{\Phi}_R(x,z) = R_{\Phi_m}(z)e^{i\{k_{xm}x - k_{zm}(z)(z-h)\}}, \qquad (25)$$

and the z components of the wave vectors

$$k_{zm}(z) = \sqrt{k^2 n^2(z) - k_{xm}^2}, \quad k_{z0} = k_z(z). \qquad (26)$$

The amplitudes of the incident and reflected fields $T_{\Phi_m}(z)$ and $R_{\Phi_m}(z)$, respectively, must be calculated with the recurrence relations (20) and (21). But now k_{z_j} has to be replaced by $k_{z_j,m} = k_{zm}(z_j)$ in all Eqs. (19)–(21). The start of the recursions for $T_{\Phi_m}(z)$ and $R_{\Phi_m}(z)$ is $j = N+1$, $T_{\Phi_m}(h_>) = T_{\Phi_m,N+1} = 1$, and $R_{\Phi_m}(h_>)$

$=R_{\Phi_m, N+1}=0$, because no reflected time-reversed state exists for $z > h$ [see the Rayleigh expansion, Eq. (6)]. In this case Eq. (19) is not necessary.

Inserting all these fields into the right side of Eq. (12)

and assuming a grating function $f(x)$ given by Eq. (13) yields after some mathematics the following expression for the coefficients B_m of the Rayleigh expansion $(K_m = m\pi/d)$:

$$B_m = e^{-iK_m g}\left\{ \frac{1}{2}\left[\left[1 + \frac{k_{zi}}{k_{zm}}\right]R(h_>) + \left[1 - \frac{k_{zi}}{k_{zm}}\right]\right](-1)^m \frac{\sin(K_m s)}{K_m d}e^{-iK_m(b_1 - b_2)}\right.$$

$$+ T(0_>)\frac{\sin(K_m g)}{K_m d}\frac{k_z^{(g)}}{k_{zm}(k_z^{(g)} + k_z^{(t)})}[(k_{zm}^{(g)} - k_z^{(t)})T_{\Phi_m}(0_>)e^{-i(k_z^{(g)} + k_{zm}^{(g)})h}$$

$$\left. -(k_{zm}^{(g)} + k_z^{(t)})R_{\Phi_m}(0_>)e^{-i(k_z^{(g)} - k_{zm}^{(g)})h}]\right.$$

$$\left. + \frac{1}{2k_{zm}d}\int_0^h \{\cdots\}\chi_m(z)dz\right\}. \tag{27}$$

Here the expression in the brackets $\{\cdots\}$ is given by

$$\{[k_z(z) + k_{zm}(z) + g_m(z)](F^{(d)}\overline{\Phi}_T)_z$$

$$-[k_z(z) + k_{zm}(z) - g_m(z)](F^{(i)}\overline{\Phi}_R)_z$$

$$+[k_z(z) - k_{zm}(z) + g_m(z)](F^{(d)}\overline{\Phi}_R)_z$$

$$-[k_z(z) - k_{zm}(z) - g_m(z)](F^{(i)}\overline{\Phi}_T)_z\}, \tag{28}$$

with the abbreviation $g_m(z)$

$$g_m(z) = \frac{i}{2}\left[\frac{\dot{k}_z(z)}{k_z(z)} - \frac{\dot{k}_{zm}(z)}{k_{zm}(z)}\right]. \tag{29}$$

A dot over a quantity means the z derivative and the notation $(\cdots)_z$ is an abbreviation for the z-dependent part of the term within the parentheses, e.g.,

$$(F^{(d)}\overline{\Phi}_T)_z = R(z)T_{\Phi_m}(z)e^{-i\{k_z(z) - k_{zm}(z)\}(z - h)}.$$

Furthermore, the function $\chi_m(z)$ is defined as follows:

$$\chi_m(z) = \dot{f}_1^{-1}(z)e^{-iK_m\{2f_1^{-1}(z) + g\}}$$

$$+ \dot{f}_2^{-1}(z)e^{iK_m\{2f_2^{-1}(z) + g\}}. \tag{30}$$

Also the special k values

$$k_{zm}^{(g)} = k_{zm}(0_>) = \{k_i^2 n^2(0_>) - k_{xm}^2\}^{1/2},$$

$$n(0_>) = 1 - (\delta + i\beta)(s + b_1 + b_2)/d,$$

$$k_z^{(g)} = k_z(0_>) = k_{z0}^{(g)},$$

and

$$k_z^{(t)} = k_z(0_<) = k_i(n^2 - \cos^2\vartheta_i)^{1/2}$$

were used in expression (27).

An important test of the result (27) is its asymptotic

behavior for rather large incidence angles (this means $\vartheta_i \gg \vartheta_c$). In this case the kinematical approximation is valid and (27) has to yield the same expression as given in Ref. 5. If Eq. (27) is expanded in the limit $\vartheta_i \gg \vartheta_c$ one obtains (for details see Ref. 55)

$$B_m \xrightarrow{\vartheta_i \gg \vartheta_c} \frac{k_{zi}}{k_{zm}}\frac{k_{zm} - k_z^{(t)}}{k_{zi} + k_z^{(t)}}\frac{1}{d}\int_0^d e^{-iq_z f(x)}e^{-2iK_m x}dx, \tag{31}$$

with $q_z = k_{zm} + k_{zi}$.

Equation (31) equals the result of the kinematical theory: The amplitudes of the scattered waves B_m are proportional to the Fourier coefficients of the function $\exp\{-iq_z f(x)\}$.[5] Of course, the prefactor in Eq. (31) does not describe the decrease of a truncation rod in the vicinity of a Bragg reflection. It correctly describes the well-known ϑ_i^{-4} decrease of the reflectivity given by the Fresnel formulas.[12,13]

But the expressions (11) and (27) are not suitable to explain x-ray-diffraction data from laterally structured surfaces quantitatively. The surface roughness as well as fluctuations of the mesoscopic grating parameters (in particular, fluctuations of the height h) have to be taken into account, too.

Now we assume a surface grating with rough bars and grooves and arbitrary intermediate regions [see Fig. 3(b)]. Both roughnesses are described by a Gaussian random distribution (i.e., an error-function density profile) with rms roughnesses σ_s on top of the bars and σ_g in the grooves, respectively.

The coefficients B_m can be calculated by averaging the integrand of Eq. (12), which means

$$B_m = \frac{1}{2dk_{zm}}\int_0^d \langle[\cdots]_{z = f(x) + \delta f(x)}\rangle dx, \tag{32}$$

with a random deviation $\delta f(x)$ from the mean shape $f(x)$ of the surface grating. This leads to the result

$$B_m = e^{-iK_m g} \left\{ \frac{1}{2} \left[\left[1 + \frac{k_{zi}}{k_{zm}} \right] R(h_>) r_s^{(-)} + \left[1 - \frac{k_{zi}}{k_{zm}} \right] r_s^{(+)} \right] (-1)^m \frac{\sin(K_m s)}{K_m d} e^{-iK_m(b_1 - b_2)} \right.$$

$$+ T(0_>) \frac{\sin(K_m g)}{K_m d} \frac{k_z^{(g)}}{k_{zm}(k_z^{(g)} + k_z^{(t)})} [(k_{zm}^{(g)} - k_z^{(t)}) r_g^{(+)} T_{\Phi_m}(0_>) e^{-i(k_z^{(g)} + k_{zm}^{(g)})h}$$

$$- (k_{zm}^{(g)} + k_z^{(t)}) r_g^{(-)} R_{\Phi_m}(0_>) e^{-i(k_z^{(g)} - k_{zm}^{(g)})h}]$$

$$\left. + \frac{1}{2k_{zm}d} \int_0^h \{ \cdots \} \chi_m(z) dz \right\} ,$$ (33)

with the roughness coefficients

$$r_s^{(\pm)} = e^{-(k_{zi} \pm k_{zm})^2 \sigma_s^2 / 2} ,$$ (34)

$$r_g^{(\pm)} = e^{-(k_z^{(g)} \pm k_{zm}^{(g)})^2 \sigma_g^2 / 2} .$$ (35)

To include the roughnesses into the recurrence relations (19), (20), and (21) the smooth Fresnel coefficients must be replaced by the rough ones.[9,15,59,63] This is done by the substitutions

$$\tilde{r}_{N+1,N} \rightarrow \tilde{r}_{N+1,N} e^{-2k_{zi}k_z(h)\sigma_s^2} ,$$

$$\tilde{t}_{N,N+1} \rightarrow \tilde{t}_{N,N+1} e^{+[k_{zi} - k_z(h)]^2 \sigma_s^2 / 2} ,$$

$$\tilde{r}_{1,0} \rightarrow \tilde{r}_{1,0} e^{-2k_z^{(g)}k_z^{(t)}\sigma_g^2} ,$$

$$\tilde{t}_{0,1} \rightarrow \tilde{t}_{0,1} e^{+[k_z^{(t)} - k_z^{(g)}]^2 \sigma_g^2 / 2} ,$$

with

$$k_z(h) = k_i \{ n^2(h) - \cos^2 \vartheta_i \}^{1/2}$$

and $n(h) = 1 - (\delta + i\beta)s/d$. It will be assumed that all other coefficients $\tilde{r}_{j+1,j}$ and $\tilde{t}_{j,j+1}$ are not affected. The field Φ_m can be calculated in the same manner for rough bars and grooves ($k_z \rightarrow k_{zm}$ and different starting points of the recurrences).

Note that Eqs. (33) and (11) do not describe the diffusely scattered intensity between the diffraction orders which is caused by the lateral structure of the surface roughnesses.[17] Due to the fact that a mesoscopic grating cannot be treated as a small perturbation of a flat surface, the DWBA fails if the eigenfunctions of a smooth surface are assumed. A calculation of the diffuse scattering cross section within the DWBA using the solution (27) as eigenfunctions is very difficult and was not done in the present work.

In principle, it is also possible to calculate the intensities of the diffraction orders within the DWBA using Eq. (27) as the averaged solution of the system. Then the grating structure acts as a perturbation of this averaged potential. Recently Baumbach et al.[57] have calculated the DWBA using this ansatz up to second order. An advantage of this theory is the inclusion of double-diffraction effects (see Ref. 35). But the disadvantage of the DWBA is that the total intensity (i.e., the energy) is not conserved,[17,58] whereas the Rayleigh expansion automatically fulfills this condition.

It turns out that not only the roughness of the bars and grooves but also fluctuations of the grating parameters have to be taken into account to explain the x-ray data quantitatively. Here, mainly fluctuations of the height h are of importance whereas fluctuations of the other parameters cannot be distinguished from the roughnesses. This does not hold for the lateral period d because a fluctuation of this quantity would cause a significant broadening of the nonspecular diffraction peaks. However, from the preparation process (see Sec. II) and the x-ray data it follows that the lateral period d is well defined and only fluctuations of s and $b_{1,2}$ may occur.

Now it is assumed that the height h itself fluctuates around a mean value $\bar{h}$ with a probability density $w(h)$. Then the measured intensity $I_m(\bar{h})$ is the convolution of $I_m(h)$ and $w(h)$:

$$I_m(\bar{h}) = \int_{-\infty}^{+\infty} I_m(h) w(\bar{h} - h) dh .$$ (36)

Therefore fluctuations of the grating height h and a bad q_z resolution δ_{q_z} of the diffractometer act in the same way: both effects are the reason for a damping of modulations in the q_z direction which are caused by interferences of scattered waves from the bars and the grooves of the grating. In the data analysis the resolution $\delta_{q_z,\text{fit}}$ was chosen as a free parameter and the ratio $\delta_{q_z,\text{fit}}/\delta_{q_z}$ is a measure for the height fluctuations. For reasons of simplicity the distribution $w(h)$ was always assumed to be Gaussian.

Thin oxide layers within the grooves and on top of the bars of the surface structure can simply be included into the calculations via the recurrence relations (19)–(21).

Furthermore, the theory presented above assumes a grating which covers the whole illuminated area of the sample surface. Due to the very small incident angles the x-ray beam also impinges on areas without a grating (especially at the edges of the samples). If ε denotes the fraction of the surface without a grating, the total reflectivity I_{ref} can be calculated in the following manner (incoherent addition of the scattering contributions):

$$I_{\text{ref}} = (1 - \varepsilon)|B_0|^2 + \varepsilon \left| \frac{k_{zi} - k_z^{(t)}}{k_{zi} + k_z^{(t)}} e^{-2k_{zi}k_z^{(t)}\sigma_s^2} \right|^2 .$$ (37)

Due to the preparation of the surfaces it is assumed that the roughness of the nonstructured regions equals the

roughness σ_s of the bars. Note that only the reflectivity is affected by regions without a grating. The intensities of the diffraction orders $(m \neq 0)$ stem from the grating and therefore they need not be modified. In principle, an oxide layer has to be included into the second term on the right-hand side of Eq. (37), too. But it turns out that $\varepsilon < 7\%$ is always valid and mainly the region of the intensity dip (see the end of this paragraph) is affected by this correction. Finally, a footprint correction of the theoretical curve using the factor $G(\vartheta_i) = (l/B)\sin\vartheta_i$ for incidence angles $\vartheta_i < \vartheta_{geo} = \arcsin(B/l)$ was done (with the length l of the sample and the width B of the beam).

Figure 4 shows the calculated reflectivity $(m=0)$ and the intensities of the first two diffraction orders $(m=1,2)$ for a trapezoidal-shaped GaAs surface grating with a lateral period $d = 15\,000$ Å, a grating height $h = 1500$ Å, and the other parameters $s = 4000$ Å, $b_1 = b_2 = 1500$ Å, and $g = 8000$ Å (see Fig. 1). In the calculation imperfections such as those mentioned above were not taken into account. The angle ϑ_{geo} was set to 1°. The dashed line in Fig. 4 is the reflectivity of a single vacuum-GaAs interface. The reflectivity of the surface grating shows a distinct dip before the critical angle ϑ_c of total external reflection of the bulk material (here $\vartheta_c = 0.307°$). This dip at the position $\vartheta_c^* \approx 0.16°$ can be explained qualitatively using the density-profile approximation. The structured surface acts like a system with a layer of smaller density on top of a denser bulk material (see, e.g., Refs. 9 and 60). Since the critical angle is proportional to the square root of the density, the critical angle ϑ_c^* of the averaged grating structure can be roughly calculated using the formula $\vartheta_c^* = \vartheta_c \sqrt{s/d}$. Inserting the values for s and d yields $\vartheta_c^* \approx 0.16°$ which equals the number obtained from Fig. 4.

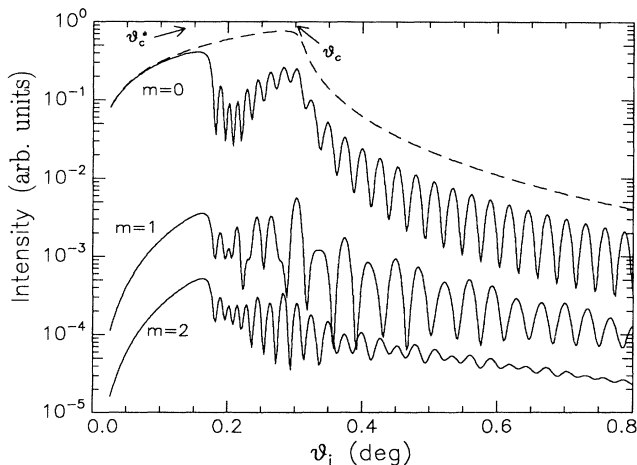The oscillations in the region $\vartheta_i > \vartheta_c^*$ are caused by the

FIG. 4. Calculated reflectivity $(m=0)$ and intensities of the first two diffraction orders for a symmetric trapezoidal-shaped surface grating (solid lines) with parameters $d = 15\,000$ Å, $h = 1500$ Å, $s = 4000$ Å, $b_1 = b_2 = 1500$ Å, and $g = 8000$ Å. No imperfections were assumed. For comparison also the reflectivity of a nonstructured smooth GaAs wafer is shown (dashed line).

grating height. The curves for $m = 1$ and 2 are qualitatively of the same structure as the reflectivity. They show the intensities of the respective diffraction orders for different incident angles [see Eqs. (10) and (11)]. But now $k_{zm}(z)$ is different from $k_z(z)$ and therefore Eq. (27) yields more complex interference terms (for details, see Ref. 55).

The experiments, in particular the measurements with the samples $S1$ and $S3$, will confirm the presented theory (see Sec. V). First a brief description of the experimental setup is given.

IV. EXPERIMENTAL SETUP

The x-ray experiments were performed using a 12-kW rotating-anode generator (Rigaku Ru 200) with copper target and a three-crystal diffractometer (TCD).[61,62] Figure 5 shows the setup. The x rays were collimated by slit 1. Then a Si(111) monochromator selects the characteristic Cu $K\alpha$ lines from the spectrum. Slit 2 only picks out the Cu $K\alpha_1$ line with a wavelength of $\lambda = 1.540\,56$ Å, which impinges onto the sample. The sample is mounted on a two-circle goniometer with an accuracy of the step motors of 0.0005°, which controls the incidence angle ϑ_i and the scattering angle $\Phi = \vartheta_i + \vartheta_f$. The detector unit contains a Si(111) analyzer and a NaI(Tl) (Canberra) scintillation counter. Vacuum tubes as well as lead shields around the system were installed to increase intensity and to reduce background radiation.

A TCD was used for the experiments because the mesoscopic length scales of the surface gratings in the x and z directions $(d \sim 1\ \mu m, h \sim 0.1\ \mu m)$ requires high resolution in the q_x and q_z directions of reciprocal space. The $|\mathbf{q}|$-dependent resolution of the given TCD is[61,62] $\delta_{q_x} = 2.9 \times 10^{-4}$ Å^{-1} and $\delta_{q_z} = 3.2 \times 10^{-4}$ Å^{-1} for a momentum transfer of $q_{zc} = 0.043$ Å^{-1} $(q_{zc} = 2k_i \sin\vartheta_c$ with the critical angle ϑ_c of GaAs). These values were used to fit our data. Note that the q_z resolution is a free parameter in our fits to take the height fluctuations into account and that these height fluctuations are described by the ratio $\delta_{q_z}/\delta_{q_z,fit}$ [see Eq. (36)].

V. MEASUREMENTS, RESULTS, AND DISCUSSION

In this section the measurements and the result of the fits are presented. In the following a symmetric trapezoid
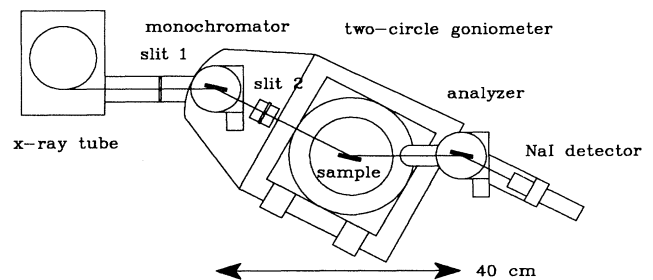

FIG. 5. Experimental setup. A three-crystal diffractometer with Si(111) monochromator and analyzer crystals was used for the x-ray measurements.

TABLE II. Results of the fits of the data concerning sample $S1$. The groove width g can be easily calculated with $g = d - s - 2b$. If no error bars are shown the respective parameter was fixed and the symbol $\sim$ means that the values of these parameters can only be roughly estimated from the calculation. The detector scan was performed at $\vartheta_i = 0.13°$.

	Reflectivity	Detector scan (Å)	First diff. order
d	15 400 Å	15 400±150	15 400 Å
s	4100±150 Å	4100	4400±200 Å
b	1800±100 Å	1800	2200±200 Å
h	1480±50 Å	1480	1500±50 Å
σ_s	12±1 Å	~ 15	14±3 Å
σ_g	35±3 Å	~ 40	31±5 Å
ε	(2.0±0.3)%		
$\delta_{q_z,\text{fit}}/\delta_{q_z}$	1.5±0.2		3.5±0.5

$(b_1 = b_2 = b)$ was always assumed as the shape of the surface grating. In a short previous paper the specular reflectivity was discussed for sample $S1$.[39] The parameters of the best fit are given in the first column of Table II. The period $d = 15\,400$ Å was obtained from off-specular detector scans using the grating formula (10). A fit of the intensities of four diffraction orders using Eq. (33) and the values of s, b, and h obtained from the reflectivity yields beside the grating period independent estimates of the roughnesses σ_s and σ_g (see second column of Table II and Ref. 55).

Figure 6 shows the measured intensities (triangles) of the first diffraction order ($m = 1$) together with the fit of the theory presented above (solid line). Because the satellites are sharp resolution-limited peaks this curve was obtained by performing detector scans over the maximum of the first diffraction order for the respective incidence angles ϑ_i. For clarity the reflectivity is also shown in Fig. 6. The parameters which were obtained from the fit of
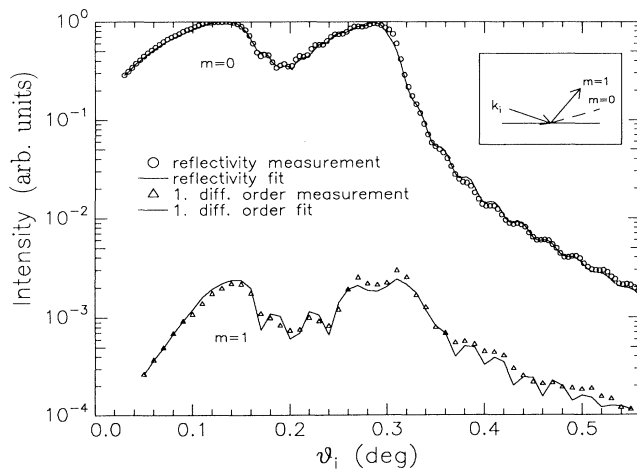
this curve are presented in Table II, too. Again the lateral period was fixed at $d = 15\,400$ Å because only the ratios s/d, b/d, and g/d enter into Eq. (33).

From the fits one can conclude that the theory is able to explain the measured data satisfactorily. Within their error bars all fits yield the same parameters for the surface grating and nearly the same roughnesses. These results are confirmed by SEM measurements. The grating height $h = 1480$ Å is very close to the calculated height from the etching time and ratio in Table I. Furthermore, the roughness σ_s of the bars is much smaller than the roughness σ_g of the grooves. This is found for all five samples and was confirmed by an atomic-force-microscope (AFM) measurement on a sample which was prepared in the same manner as the samples $S1-S5$. The AFM picture shows that the rms roughness of the grooves is more than twice as big as the respective roughness on top of the bars. One possible reason is the preparation process. During the etching the bars are
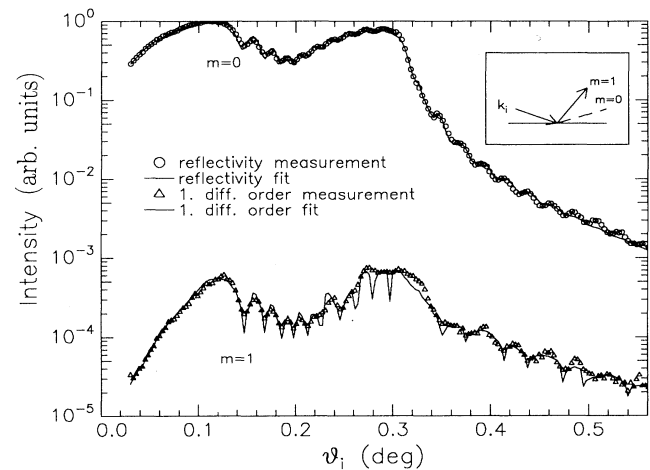

FIG. 6. Intensity of the first diffraction order ($m = 1$) for sample $S1$ dependent on the incidence angle ϑ_i. The triangles represent the measurement and the line is the best fit using the theory given in the text. For comparison the reflectivity ($m = 0$) is also shown (open circles).

FIG. 7. Intensity of the first diffraction order ($m = 1$) for sample $S3$ dependent on the incidence angle ϑ_i. The triangles represent the measurement and the line is the best fit using the theory given in the text and the parameters of Table III. For comparison above the reflectivity ($m = 0$) is also shown (open circle).

covered with the photoresist so that the smooth MBE GaAs is not affected by the sample preparation.

The parameter ε shows that there are 2% nongrating contributions to the reflectivity. This value seems to be reasonable because optical experiments in the region of visible light show that only the edges of the sample are not covered with a grating. Furthermore, there is a big difference between the results for $\delta_{q_z, \text{fit}} / \delta_{q_z}$ (see Table II). This could be a hint that the description of the height fluctuations using Eq. (36) is too simple.

Figure 7 contains the reflectivity and the intensity of the first diffraction order for sample $S3$. The reflectivity measured over a larger q_z range is presented in Ref. 63. Figure 8 shows a detector scan for fixed incidence angle $\vartheta_i = 0.13°$. The shoulder at $\Phi = 0.43°$ is the so-called Yoneda peak (see Refs. 17 and 64). This peak in the diffuse scattering occurs if the incident or exit angle equals the critical angle of the bulk material. In this work only the locations of the diffraction orders as well as their intensities are of interest. The diffusely scattered intensity between the diffraction orders cannot be described by the theory of Sec. III.

Table III contains the fit results for the various scans. The first column gives the result of the best fit of the reflectivity. Due to the longer etching time the height h and the width of the intermediate regions b of the surface grating are larger than the respective parameters of sample $S1$ whereas the width s becomes smaller. The roughnesses and imperfections are of the same magnitude as obtained for $S1$. The fits of the four diffraction orders (grating parameters fixed, only d and the roughnesses are free parameters) and the fit of the first diffraction order as a function of the incidence angle (see Fig. 7) lead to the same roughnesses and mesoscopic grating parameters.

Although rather good fits are obtained for the data of the samples $S1$ and $S3$ (see Figs. 6 and 7) it should clearly be mentioned that for larger incidence angles ϑ_i the height oscillations are damped out in the calculated curve whereas in the measurement they are still visible. There are several possible reasons for this behavior. First, it is possible that the density-profile approximation breaks down in this region. But this seems not to be the reason because Eq. (31) leads to the correct kinematical limit, i.e., the limit of large incidence angles. Another point is
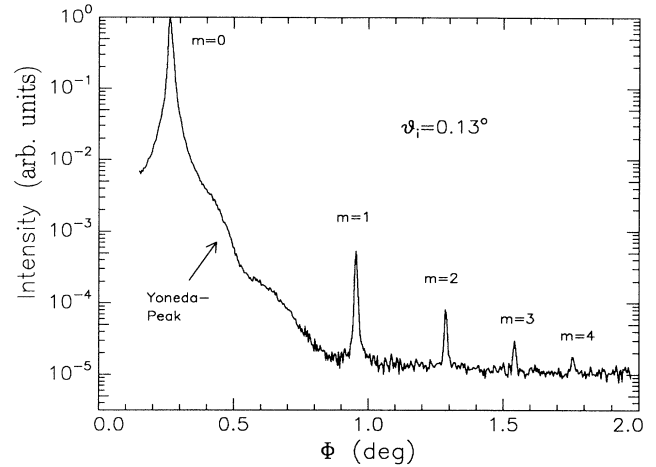

FIG. 8. Detector scan of sample $S3$ for the fixed incidence angle $\vartheta_i = 0.13°$. The "peak" at the position $\Phi = \vartheta_i + \vartheta_f \approx 0.43°$ is the so-called Yoneda peak; a common feature in the structure of the diffuse background.

the roughness distribution which was assumed (here a Gaussian for both roughnesses σ_s and σ_g). Maybe another distribution should be chosen. The work of Bahr et al.[9] shows that x-ray reflectivity is very sensitive to the particular distribution which is used to model the influence of the microscopic roughness on the specular reflected intensity. Finally, it is possible that the parameters $\delta_{q_z, \text{fit}}$ and ε do not describe the imperfections of the sample surface correctly. All three reasons might be the source for this damping of the height oscillations and a clear decision which reason is the most important one is not possible. But the SEM pictures give small hints that the modeling of the height fluctuations assuming a Gaussian distribution $w(h)$ in Eq. (36) is too simple because there seem to be regions where the height h is well defined and other regions where a fluctuation is slightly visible.

In comparison to $S1$ and $S3$ a completely different behavior is obtained for $S2$. Figure 9 shows the measured reflectivity (open circles) and the fitted curve (solid line) for this sample. For clarity the inset shows the re-

TABLE III. Results of the fits of the data concerning sample $S3$. If no error bars are shown the respective parameter was fixed and the symbol $\sim$ means that the values of these parameters can only be roughly estimated from the calculation. The detector scan was done at $\vartheta_i = 0.13°$.

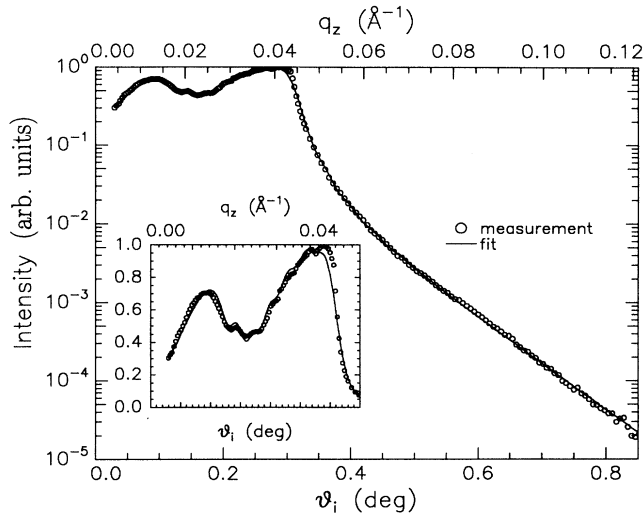|	Reflectivity	Detector scan (Å)	First diff. order
d	15 400 Å	15 400±100	15 400 Å
s	2800±100 Å	2800	3000±200 Å
b	2400±150 Å	2400	2200±200 Å
h	1790±40 Å	1790	1800±50 Å
σ_s	14±1 Å	~20	19±3 Å
σ_g	34±4 Å	~45	39±4 Å
ε	(2.6±0.4)%		
$\delta_{q_z, \text{fit}} / \delta_{q_z}$	1.5±0.2		2.5±0.5

FIG. 9. Reflectivity of sample $S2$. The open circles represent the measurement and the solid line is the best fit with the parameters given in Table IV below. For clarity the inset shows the region of the critical angle $0° \leq \vartheta_i \leq 0.35°$ on a linear intensity scale.

FIG. 10. Reflectivity of sample $S4$. The open circles represent the measurement and the solid line is the best fit with the parameters given in Table V. For clarity the inset shows the region of the critical angle $0° \leq \vartheta_i \leq 0.35°$ on a linear intensity scale.

gion before the critical angle on a linear intensity scale. Now no height oscillations for $q_z > q_{zc}$ are visible and the dip before the critical angle is not as pronounced as observed for the samples $S1$ and $S3$.

Table IV contains the results of the fits for the reflectivity (left column) and one detector scan with $\vartheta_i = 0.29°$ (second column) which is not shown here.[55] Although this sample was prepared in the same manner as $S1$ the parameters obtained are quite different. The height $h = 1200$ Å (from the etching time $h \approx 1500$ Å was expected) which results from the fits of the x-ray data of $S2$ suggests that these differences are caused by the photoresist which has covered the GaAs substrate. Maybe this photoresist was inhomogeneous and the subsequent etching process leads to the observed differences. The weak oscillations in the reflectivity are also a hint that the grating is not very well defined. This is confirmed by

the fit parameters ε and $\delta_{q_z,\mathrm{fit}}/\delta_{q_z}$ which determine the imperfections of the grating. The obtained values and the roughnesses σ_s and σ_g are larger than the respective numbers for $S1$ and $S3$.

After the x-ray measurements a SEM investigation of this sample was done. The expected imperfections of the grating are clearly visible because the pictures show a grating with well-defined spacing d but the width s of the bars is strongly varying over the sample surface (for de-

TABLE IV. Results of the fits from the reflectivity and one detector scan at $\vartheta_i = 0.29°$ for sample $S2$. Again the values without error bars are fixed and the sign $\sim$ means that these numbers are only rough estimates with rather large error bars. The right column contains the values which were obtained from the analysis of SEM pictures.

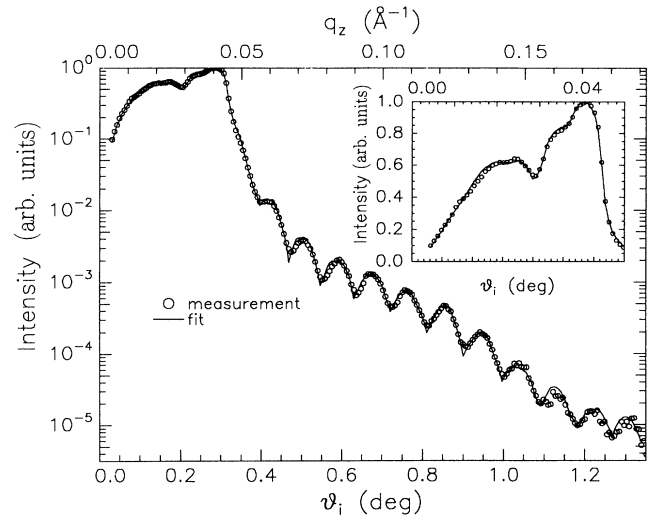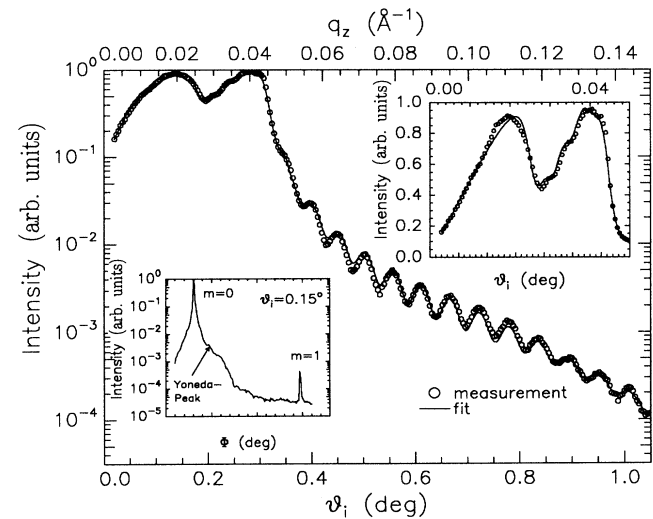|	Reflectivity	Detector scan (Å)	SEM (Å)
d	15 400 Å	15 400±100	~15 000
s	1500±400 Å	1500	~1500
b	1700±300 Å	1700	~1500
h	1200±100 Å	1200	~1500
σ_s	18±1 Å	~20	
σ_y	44±4 Å	~40	
ε	(7.2±0.5)%		
$\delta_{q_z,\mathrm{fit}}/\delta_{q_z}$	2.5±0.8		

FIG. 11. Reflectivity of sample $S5$. The open circles represent the measurement and the solid line is the best fit with the parameters given in Table V. For clarity the upper right inset shows the region of the critical angle $0° \leq \vartheta_i \leq 0.35°$ on a linear intensity scale. The lower left inset shows a detector scan for fixed $\vartheta_i = 0.15°$. The specular peak is denoted by $m = 0$ and the first diffraction order by $m = 1$.

TABLE V. Results of the fits and the SEM pictures for $S4$ and $S5$. The values without error bars are fixed and the sign $\sim$ means that these numbers are only rough estimates with rather large error bars. The right column contains the values for $S5$. The value for the grating period d was calculated only from the position of the first diffraction order (see lower inset of Fig. 11). Note that the density $\bar{\rho}$ of the oxide layer was set to $\bar{\rho}=0.9\,\rho_{GaAs}$

| | | $S4$ | | $S5$ |
	Reflectivity	Detector scan (Å)	SEM (Å)	Reflectivity
d	5900 Å	5900±50	~6000	5900±500 Å
s	1630±50 Å	1630	~1500	1400±40 Å
b	640±30 Å	640	~750	940±40 Å
h	480±10 Å	480	~500	730±10 Å
σ_s	10±1 Å	~10		7±1 Å
σ_g	29±3 Å	~30		19±2 Å
$\tilde{h}$	44±8 Å			52±10 Å
ε	(3.1±0.2)%			(1.8±0.3)%
$\delta_{q_z,\text{fit}}/\delta_{q_z}$	1.6±0.3			1.4±0.2)

tails, see Ref. 55). The parameters obtained from the SEM measurements are given in the last column of Table IV. It can be seen that a rather good agreement between the x-ray data and the SEM investigations is achieved but it should also be mentioned that the errors are rather big.

In contrast to the first three samples the grating period of $S4$ and $S5$ was $d=5900$ Å. Figures 10 and 11 and Table V show the reflectivities and the parameters obtained from the fits of these curves and an additional detector scan (not shown here, see Ref. 55). Both reflectivities are quite similar to those of the samples $S1$ and $S3$ but an additional modulation due to an oxide layer is observed. We model this oxide layer by introducing a thin layer of the density $\bar{\rho}=0.9\rho_{GaAs}$ (see, e.g., Refs. 65 and 66) on top of the bars. This particular layer of thickness $\tilde{h}$ can be simply included into the recurrence relations (19)–(21) by modifying the grating-vacuum interface in the appropriate manner.

Of course the grating parameters obtained for $S4$ and $S5$ are different from the parameters of $S1$ and $S3$. But one can say that both gratings are also well defined because they show pronounced x-ray-scattering curves. The roughnesses of the bars and grooves are a little smaller than those of $S1$ and $S3$ but in contrast to $S1$ and $S3$ the aforementioned oxide layer of roughly $\tilde{h}\approx 50$ Å has to be taken into account. The rms roughness σ_s is now the roughness of the oxide-vacuum interface. An oxide layer within the grooves is also expected. But this layer seems not to be very thick or its influence on the diffracted intensity is so weak that it cannot be distinguished from the roughness described by the parameter σ_g. This may also be the reason why an oxide layer was not detected for $S1$–$S3$. Furthermore, the q_z region for the measurements of the first three samples was so small that the additional modulation caused by a thin layer of thickness $\tilde{h}\sim 50$ Å cannot be detected.

After the x-ray investigations a SEM picture was taken for sample $S4$. It leads to the same mesoscopic grating parameters as given in Table V (for details, Ref. 55). Additionally, the picture shows that the grating is well defined. This conclusion can also be made from the

values of the parameters of the height fluctuations and the nongrating contributions which are not very big.

Finally, all values obtained for $S1$–$S5$ are compared with the results of wide-angle-scattering data. For all samples, truncation rods[3,4] in the vicinity of the 004 GaAs bulk Bragg reflection are measured and fitted with a simple kinematic model. This is described in detail in Ref. 5. It turns out that the parameters obtained from the small-angle measurements are in very good agreement with the results of the wide-angle data.

VI. CONCLUSIONS AND OUTLOOK

In summary, we have shown that laterally structured surfaces can be quantitatively investigated within the region of total external reflection by the nondestructive x-ray-scattering technique. We have calculated the scattered intensities in a dynamical way, only assuming that the grating can be replaced in a zeroth-order approximation by a special kind of layer system. Measurements and calculations show that the presented theory is valid up to wavelengths of $\lambda=10$ Å.[55,63] Due to the large incidence angles the density-profile approximation breaks down for wavelengths in the vacuum-ultraviolet and soft-x-ray regimes.

Our measurements and calculations are not only able to yield the mesoscopic grating parameters, but also a feeling for the imperfections of surface gratings is obtained. Roughnesses, height fluctuations, nonstructured regions, and oxide layers contribute to the scattering too, and were included into the theory in a straightforward manner. Furthermore, SEM measurements as well as wide-angle x-ray data confirm the results obtained.

[1]H. Dosch, *Critical Phenomena at Surfaces and Interfaces (Evanescent X-Ray and Neutron Scattering)*, Springer Tracts in Modern Physics Vol. 126 (Springer-Verlag, Berlin, 1992).

[2]R. W. James, *The Optical Principles of the Diffraction of X-Rays* (Ox Bow Press, Woodbridge, 1982).

[3]S. R. Andrews and R. A. Cowley, J. Phys. C **18**, 6427 (1985).

[4]I. K. Robinson, Phys. Rev. B **33**, 3830 (1986).

[5]M. Tolan, W. Press, F. Brinkop, and J. P. Kotthaus, J. Appl. Phys. **75**, 7761 (1994).

[6]M. Born and E. Wolf, *Principles of Optics*, 2nd ed. (Pergamon, Oxford, 1964).

[7]L. G. Parrat, Phys. Rev. **95**, 359 (1954).

[8]F. Abelés, Ann. Phys. (Paris) **5**, 596 (1950).

[9]D. Bahr, W. Press, R. Jebasinski, and S. Mantel, Phys. Rev. B **47**, 4385 (1993).

[10]S. Garoff, E. B. Sirota, S. K. Sinha, and H. B. Stanley, J. Chem. Phys. **90**, 7505 (1989).

[11]M. Stamm, G. Reiter, and K. Kunz, Physica B **173**, 35 (1991).

[12]J. Lekner, *Theory of Reflection* (Nijhoff, Dordrecht, 1987).

[13]J. Lekner, Physica B **173**, 99 (1991).

[14]P. Beckmann and A. Spizzichino, *The Scattering of Electromagnetic Waves From Rough Surfaces* (Pergamon, New York, 1963).

[15]L. Névot and P. Croce, Rev. Phys. Appl. **15**, 761 (1980).

[16]A. V. Andreev, A. G. Michette, and A. Renwick, J. Mod. Opt. **35**, 1667 (1988).

[17]S. K. Sinha, E. B. Sirota, S. Garoff, and H. B. Stanley, Phys. Rev. B **38**, 2297 (1988).

[18]S. K. Sinha, Physica B **173**, 25 (1991).

[19]S. K. Sinha, M. K. Sanyal, S. K. Satija, C. F. Majkrzak, D. A. Neumann, H. Homma, S. Szpala, A. Gibaud, and H. Morkoc, Physica B **198**, 72 (1994).

[20]R. Pynn, Phys. Rev. B **45**, 602 (1992).

[21]R. Pynn and S. Baker, Physica B **198**, 1 (1994).

[22]D. K. G. de Boer, Phys. Rev. B **44**, 498 (1991).

[23]D. K. G. de Boer, Phys. Rev. B **49**, 5817 (1994).

[24]M. K. Sanyal, S. K. Sinha, A. Gibaud, S. K. Satija, C. F. Majkrzak, and H. Homma, in *Surface X-Ray and Neutron Scattering*, edited by H. Zabel and I. K. Robinson, Springer Proceedings in Physics Vol. 61 (Springer, Berlin, 1992), pp. 91–94.

[25]V. Holý, J. Kubêna, I. Ohlídal, K. Lischka, and W. Plotz, Phys. Rev. B **47**, 15 896 (1993).

[26]V. Holý and T. Baumbach, Phys. Rev. B **49**, 10 668 (1994).

[27]L. B. Lurio, T. A. Rabedeau, P. S. Pershan, I. F. Silvera, M. Deutsch, S. D. Kosowsky, and B. M. Ocko, Phys. Rev. Lett. **68**, 2628 (1992).

[28]V. V. Aristov, A. I. Erko, A. Yu. Nikulin, and A. A. Snigirev, Opt. Commun. **58**, 300 (1986).

[29]V. V. Aristov, A. Yu. Nikulin, A. A. Snigirev, and P. Zaumseil, Phys. Status Solidi A **95**, 81 (1986).

[30]V. V. Aristov, U. Winter, A. Yu. Nikulin, S. V. Redkin, A. A. Snigirev, P. Zaumseil, and V. A. Yunkin, Phys. Status Solidi A **108**, 651 (1988).

[31]A. T. Macrander and S. E. G. Slusky, Appl. Phys. Lett. **56**, 443 (1990).

[32]L. Tapfer and P. Grambow, Appl. Phys. A **50**, 3 (1990).

[33]L. Tapfer, G. C. La Rocca, H. Lage, R. Crigolari, P. Grambow, A. Fischer, D. Heitmann, and K. Ploog, Surf. Sci. **267**, 227 (1992).

[34]P. van der Sluis, J. J. M. Binsma, and T. van Dongen, Appl. Phys. Lett. **62**, 3186 (1993).

[35]M. Gailhanou, G. T. Baumbach, U. Marti, P. C. Silva, F. K. Reinhart, and M. Ilegems, Appl. Phys. Lett. **62**, 1623 (1993).

[36]Q. Shen, C. C. Umbach, B. Weselak, and J. M. Blakely, Phys. Rev. B **48**, 17 967 (1993).

[37]V. Holý, L. Tapfer, E. Koppensteiner, G. Bauer, H. Lage, O. Brandt, and K. Ploog, Appl. Phys. Lett. **63**, 3140 (1993).

[38]D. Maystre, in *Rigorous Vector Theories of Diffraction Gratings*, Progress in Optics XXI, edited by E. Wolf (North-Holland, Amsterdam, 1984).

[39]M. Tolan, G. König, L. Brügemann, W. Press, F. Brinkop, and J. P. Kotthaus, Europhys. Lett. **20**, 223 (1992).

[40]F. Brinkop, Ph.D. thesis, LMU München, 1993.

[41]W. Hansen, in *Quantum Coherence in Mesoscopic Systems*, edited by B. Kramer (Plenum, New York, 1991).

[42]W. Hansen, J. P. Kotthaus, and U. Merkt, in *Nanostructured Systems*, edited by R. K. Willardson, A. C. Beer, and E. R. Weber, Semiconductors and Semimetals Vol. 35 (Academic, San Diego, 1992), pp. 279–380.

[43]D. Heitmann and J. P. Kotthaus, Phys. Today **46** (6), 56 (1993).

[44]W. Jark, Opt. Commun. **60**, 201 (1986).

[45]G. Schmahl and D. Rudolph, in *Holographic Diffraction Gratings* Progress in Optics XIV, edited by E. Wolf (North-Holland, Amsterdam, 1976).

[46]Yu. A. Basov, T. L. Pravdivtseva, A. A. Snigirev, M. Belakhovsky, P. Dhez, and A. Freund, Nucl. Instrum. Methods Phys. Res. Sect. A **308**, 366 (1991).

[47]V. V. Aristov, Yu. A. Basov, A. A. Snigirev, and V. A. Yunkin, Nucl. Instrum. Methods Phys. Res. Sect. A **308**, 413 (1991).

[48]T. Demel, D. Heitmann, P. Grambow, and K. Ploog, Superlatt. Microstruct. **9**, 285 (1991).

[49]J. A. Lebens, C. S. Tsai, K. J. Vahala, and T. F. Kuech, Appl. Phys. Lett. **56**, 2642 (1990).

[50]F. Brinkop, W. Hansen, J. P. Kotthaus, and K. Ploog, Phys. Rev. B **37**, 6547 (1988).

[51]U. Merkt, Phys. Bl. **6**, 509 (1991).

[52]B. Meurer, D. Heitmann, and K. Ploog, Phys. Rev. Lett. **68**, 1371 (1992).

[53]L. Rayleigh, *The Theory of Sound* (Dover, New York, 1945), Vol. 2.

[54]D. Maystre and M. Cadilhac, J. Mod. Opt. **26**, 2201 (1985).

[55]M. Tolan, Ph.D. thesis, Kiel University, 1993.

[56]M. Tolan, D. Bahr, J. Süßenbach, W. Press, F. Brinkop, and J. P. Kotthaus, Physica B **198**, 55 (1994).

[57]G. T. Baumbach, M. Gailhanou, P. Mikulik, and M. Bessiere (unpublished).

[58]D. K. G. de Boer, Phys. Rev. B (to be published).

[59]B. Vidal and P. Vincent, Appl. Opt. **23**, 1794 (1984).

[60]S. M. Heald, H. Chen, and J. M. Tranquada, Phys. Rev. B **38**, 1016 (1988).

[61]L. Brügemann, Ph.D. thesis, Kiel University, 1989.

[62]L. Brügemann, R. Bloch, W. Press, and M. Tolan, Acta. Crystallogr. Sect. A **48**, 688 (1992).

[63]W. Press, D. Bahr, M. Tolan, B. Burandt, M. Müller, P. Müller-Buschbaum, V. Nitz, and J. Stettner, Physica B **198**, 42 (1994).

[64]Y. Yoneda, Phys. Rev. **131**, 2010 (1963).

[65]R. Bloch, Ph.D. thesis, Kiel University, 1990.

[66]R. Bloch, L. Brügemann, W. Press, M. Tolan, K.-M. Behrens, J. Olde, and M. Skibowski, J. Phys. C **4**, 4221 (1992).